Heliyon 10 (2024) e26327

Contents lists available at ScienceDirect

Heliyon

journal homepage: www.cell.com/heliyon

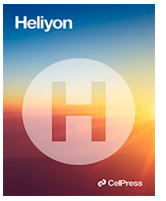

Research article

Investigation of the driving voltage on the high performance flexible ATF-ECDs based on PET/ITO/NiO_X/$LiTaO_3$/WO_3/ITO

Jinhong Ye [a,1], Mingtao Chen [a,1], Hanyu Lu [a], Hongbing Zhu [a,b], Meixiu Wan [a,b,*], Kai Shen [a,b], Yaohua Mai [a,b]

[a] College of Information Science and Technology, Jinan University, Guangzhou, 510632, PR China
[b] Institute of New Energy Technology, College of Physics and Optoelectronic Engineering, Jinan University, Guangzhou, 510632, PR China

ARTICLE INFO

Keywords:
Flexible ATF-ECDs
Electrochromic performance
NiO_X thin films

ABSTRACT

High performance flexible all-thin-film electrochromic devices (ATF-ECDs) have been fabricated and systematically investigated by operating with different driving voltages during the electrochromic processes. The device structure (cross-section) and material properties of some main functional layers were presented and analysed. The electrochromic properties including kinetic and spectral tests were systematically investigated through combining chronoamperometry, cyclic voltammetry measurements and optical measurements. In addition, the open circuit memory measurement was also carried out. A much higher driving voltage might lead to a current leakage inside the device during coloring process. A proper driving voltage is needed for achieving high device performances. More details were widely described and deeply discussed.

1. Introduction

Electrochromic devices (ECDs) have a promising application in the future smart window of buildings and vehicles [1–3]. All-thin-film ECDs (ATF-ECDs) based on lithium ion (Li^+) transfer are much stable and controllable as compared to the ones based on the proton (H^+) transfer. Normally the protons come from the absorbed water (H_2O) in the environment, which is variable and uncontrollable for the humidity. For this kind of ATF-ECDs, the inner proton concentration might be variable and then strongly affect the electrochromic performance of the devices. The tantalum pentoxide (Ta_2O_5) [4–7], niobium pentoxide (Nb_2O_5) [8] and zirconium dioxide (ZrO_2) [9,10] are normally used as the solid electrolyte (SE) layers with the H^+ inside. Differently, the Li^+ based lithium tantalate ($LiTaO_3$) [11–14] and lithium niobate ($LiNbO_3$) [15–18] SE materials are employed in ATF-ECDs to get good electrochromic performances. In addition, the multiple ions like Li^+ and Al^{3+} were reported to work as conjugated transfer ions in some special SE layers for applications in ATF-ECDs [19,20]. The related transfer mechanism of multiple ions in these SE layers seems much complicated. The Li^+ has a small radius as compared to other transfer ions except protons and might have a promising mobility. Thus, the Li^+ based SE materials receive much attraction for applications in ATF-ECDs. These kinds of materials are normally ceramic and prepared by radio frequency (RF) magnetron sputtering technology when ATF-ECDs are prepared [14,16]. However, the deposition rate is rather low for RF sputtering as compared to that for direct current (DC) reactive magnetron sputtering from the metal targets for preparing the proton-based metal oxide SE materials like Ta_2O_5 and ZrO_2. At the same time, in order to keep a good electron blocking

* Corresponding author. College of Information Science and Technology, Jinan University, Guangzhou 510632, PR China.
E-mail address: wanmeixiu1981@jnu.edu.cn (M. Wan).
[1] Co-first authors.

https://doi.org/10.1016/j.heliyon.2024.e26327
Received 12 November 2023; Received in revised form 7 January 2024; Accepted 12 February 2024
Available online 21 February 2024

and achieve better device performances, the thickness of Li^+ based SE layers required much high of more than 440 nm and even up to 1250 nm [14]. The required deposition time might be more than 180 min [11]. As a result, the cost-efficient ATF-ECDs seem hard to be obtained and their industrial development and commercial expansion might be held back. Some researchers employed Ta_2O_5/Li^+ based SE layer/Ta_2O_5 complex SE layers to decrease the thickness of Li^+ based SE layer for applications in the ATF-ECDs and at the same time to achieve better device performances [16,19]. There still are a few noticed points: (1) the complex SE layers added the preparation complexity in not only the process but also the preparation set-up; (2) the inner ionic transportation mechanism is also complex and hard to analyse since more interfaces are added and then multiple ion transfer and/or ionic exchange (Li^+ and H^+) in-between different SE layers might take places. In the future, the much thinner Li^+ based SE layer is needed for application in the ATF-ECDs.

Differing from the quasi-solid electrolytes (QSEs) (like Lithium perchlorate ($LiClO_4$)-Propylene carbonate (PC) + poly(methyl methacrylate (PMMA)) based ECDs [21,22], the total thickness of ATF-ECDs is normally about 1 μm. The inner ionic concentration and conductivity (at about 10^{-8} S/cm) of the ATF-ECDs is much lower than those of QSE based ECDs, whose conductivity is about (10^{-4} S/cm) [23]. As a result, the applied voltage would have profound influences on the carrier transfer (including ions and electrons) as well as the resulting electrochromic properties of the ATF-ECDs. Liu et al. [17] studied the dynamic behaviors of the inorganic all-solid-state ECD with seven superimposed layers of glass/ITO/NiOx/Ta_2O_5/$LiNbO_3$/Ta_2O_5/WO_3/ITO by applying different voltages. They attributed the imbalance of the transferred charges during bleaching and coloring processes to the trapped Li^+ ions in WO_3 layers. As a matter of fact, they employ a relatively low voltage during the coloring process. When a much higher voltage is imposed, the ATF-ECDs will present different electrical and electrochemical properties.

As compared to rigid ATF-ECDs on glass substrates, the flexible ATF-ECDs on plastic substrates (polyethylene terephthalate (PET), polyethylene naphthalate (PEN), etc.) have a few advantages as follows:(1) weight light, (2) flexible, (3) portability, (4) roll-to-roll process with low production costs, (5) easier to be transported (6) easier to be installed in the existing glazing [1–3]. Li^+ transferred flexible ATF-ECDs might have a promising application in the future smart windows of buildings and vehicles in terms of controllable preparation process and stability in practical applications as mentioned above. Much thinner functional layers (including ion storage (IS) and SE layers) integrated into the flexible substrate have some advantages such as higher cost-efficiency, less cracks taking place during bending to some extents (high flexibility), faster ion transfer and highly electrical-optical responses for these flexible ATF-ECDs, which deserve to be investigated. Even though a few researchers reported this kind of flexible ATF-ECDs, their electrochromic properties could be improved further [11].

In this study, the comprehensive electrochromic performances of our optimized flexible ATF-ECDs are systematically investigated by applying different driving voltages. The device structure and related functional layers are also presented. Much thinner functional layers have been prepared and employed in the flexible ATF-ECDs and good electrochromic performances are also obtained. Furthermore, the influence of the applied voltages on the device performances is analysed and discussed in details.

2. Experiment details

Flexible ATF-ECDs with the stacked structure of PET/ITO/NiO_X/$LiTaO_3$/WO_3/ITO were fabricated on PET substrates and optimized by employing an 100 nm thick NiO_X as the IS layer, a 200 nm thick $LiTaO_3$ (200 nm) as the SE layer and a 300 nm thick WO_3 as CE layer as well as bottom and top ITO electrodes with the same thickness (120 nm). All functional layers were successively prepared by magnetron sputtering. The NiO_X and $LiTaO_3$ layers of the ATF-ECDs were prepared in our 3-target magnetron sputtering system with the round cathodes of 76.2 mm in diameter while the ITO electrodes and WO_3 EC layer were prepared in our in-line magnetron sputtering system with rectangle cathodes (240 mm (length) × 80 mm (width)). The NiO_X and WO_3 layers were prepared by DC reactive magnetron sputtering from the Ni and W targets, respectively. The NiO_X layer was prepared in the oxide mode zone while WO_3 layer were sputtered at the deflection point in the discharge voltage-oxygen (O_2) flux curves, which is obtained with a target voltage monitoring and controlling system [24]. The bottom and top ITO electrodes were prepared by RF magnetron sputtering from an In_2O_3:SnO_2 (90:10 wt%) ceramic target. The $LiTaO_3$ SE layer was also prepared by RF magnetron sputtering from a $LiTaO_3$ ceramic target, where the deposition rate and film thickness were monitored and controlled with a quartz crystal oscillator set-up. The detailed parameters for these optimized functional layers are listed in Table 1 and could be referred to our earlier works [7,24–27]. Different driving voltages during coloring processes between −2 V and −3 V were imposed on the optimized flexible ATF-ECDs to investigate kinetic behaviours in electrical, electrochemical and optical properties.

The Bruker Dektak XT surface profiler was used to test the film thickness. The structural characterization was performed with the Bruker D8 Advance x-ray diffractometer (XRD) in a theta-2 theta test mode using Cu $K_{\alpha 1}$ x-ray incident radiation (1.54056 Å). The

Table 1
The deposition conditions of all functional layers in the optimized flexible ATF-ECDs.

Functional layer	Sputtering type	Discharge power (W)	Target material	Working pressure (Pa)	Ar flux (sccm)	O_2 flux (sccm)	d (nm)
ITO	RF	450	In_2O_3:SnO_2 (90:10 wt %)	0.3	30	0	120
NiO_X	DC	200	Ni	2	40	15	100
$LiTaO_3$	RF	200	$LiTaO_3$	3	40	0	200
WO_3	DC	200	W	4	40	4.5	300

morphologies of the all functional thin films were characterized by the scanning electronic microscopy (SEM) (FEI NovaNano 450 or FEI Apreo) while the cross-sections of the flexible ATF-ECDs were measured using another SEM equipment (FEI Apreo). The internal chemical properties were tested with the x-ray photoelectron spectroscopy (XPS, Thermo Scientific™ K-Alpha™) using the Al K_α x-ray radiation in a constant analyzer energy mode. The optical properties including the total transmittance (TT) and total reflectance (TR) spectra of the functional layers were measured by a Cary 5000 UV–Vis–NIR spectrophotometer. The kinetic tests for the TT at a specific wavelength (@600 nm) were also carried out for the flexible ATF-ECDs and related functional layers during the synchronous chronoamperometry (CA) or cyclic voltammetry (CV) measurement processes by a Zahner Zennium electrochemical station. Normally, the CA measurements of the flexible ATF-ECDs were carried out under different voltages between −2 V and −3 V during coloring steps while at the same voltage of 3 V during bleaching steps with the same durations of 30 s for both electrochromic steps. The voltage was linearly swept from −2 eV to 3 eV with a scan rate of 50 mV/s during the CV measurements. Moreover, the ionic conductivity of the $LaTaO_3$ SE layer was measured by the electrochemical impedance spectroscopy (EIS) method under a driving voltage of 50 mV with an AC mode in the Zahner Zennium electrochemical station.

3. Results and discussions

Fig. 1(a) shows the schematic configuration of the flexible ATF-ECDs (PET/ITO/NiO_X/$LiTaO_3$/WO_3/ITO). Fig. 1(b) shows the cross-section of the flexible ATF-ECDs stacked with five functional layers i.e. a 120 nm thick ITO bottom electrode, a 100 nm thick NiO_X IS layer, a 200 nm thick $LiTaO_3$ SE layer, a 300 nm thick WO_3 CE layer, a 120 nm thick top ITO electrode. Fig. 1(c–f) exhibits the corresponding morphologies of these functional layers. As shown in Fig. 1(f), the bottom ITO electrode deposed on the PET substrate shows much compacted and smooth morphology with a relatively low sheet resistance of about 35 Ω/while the top ITO electrode will follow the morphologies of previous functional layers.

The 100 nm thicker NiO_X shows a relatively smooth and compacted morphology with small particles on the surface as shown in Figs. 1(e) and Fig. 2 (a). Even though the NiO_X layer has a relatively low optical modulation as a supplementary EC functional layer in the ATF-ECDs, it plays a very important role in device performances as IS layer. Its material properties including morphology, crystal structure, optical properties and chemical compositions have been deeply investigated [25,26]. The optimized NiO_X IS layer reactively sputtered on PET substrate at room temperature exhibits a very small (111) diffraction peak at 2-theta of about 37.2° according to the Joint Committee on Powder Diffraction Standard (JCPDS) card # 47–1049 as shown in Fig. 2 (b). Wen et al. [28] reported that the single NiO_X thin films with the (111) preferred lattice plane of a higher Ni density exhibited larger optical modulation as compared to that of NiO_X thin films with the (100) preferred lattice plane. In addition, the as-prepared NiO_X thin film on the PET/ITO substrates has a relatively low transmission as shown in Fig. 2 (c), which is mainly due to the inner Ni_2O_3 phase with a lower bandgap as compared to that of NiO. The NiO_X thin films prepared at the oxide mode would generate the Ni vacancies inside and consequently the Ni^{2+} would be converted into Ni^{3+} in order to keep the electrical neutrality inside the thin films. It is confirmed by the XPS results in the inset of Fig. 2 (d). It is found that the [Ni^{3+}]/[Ni^{2+}] ratio could be up to 55.5/45.5, which implies that Ni vacancies abound inside the NiO_X. These vacancies would be good for the carrier transfer as well.

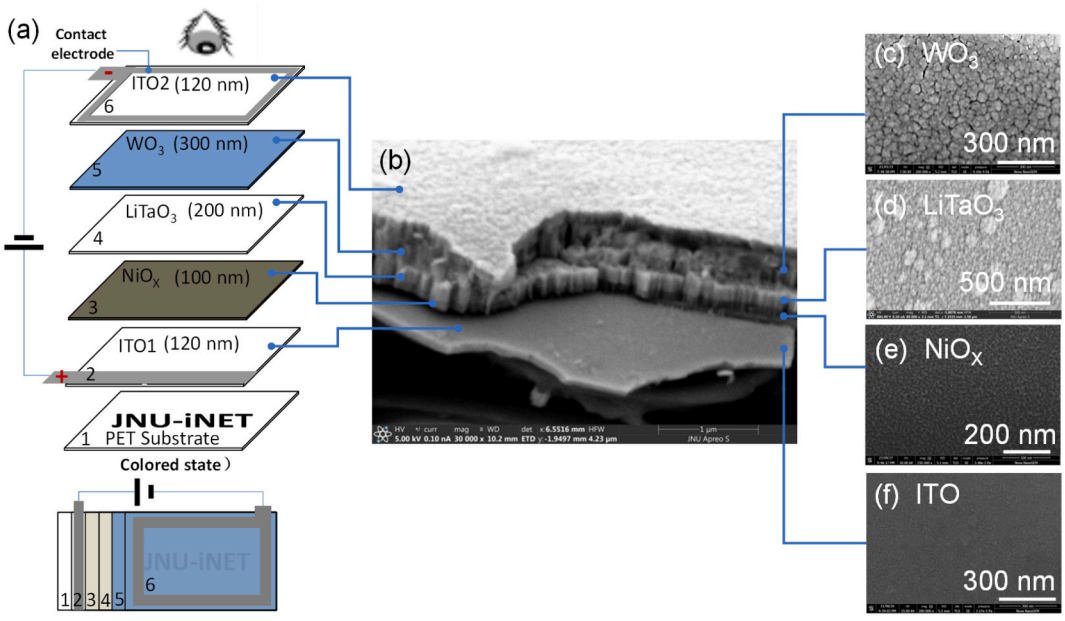

Fig. 1. The schematic configuration of the flexible ATF-ECD (a), the cross-sectional structure of the optimized devices (b) and the morphologies of the functional layers (c–f).

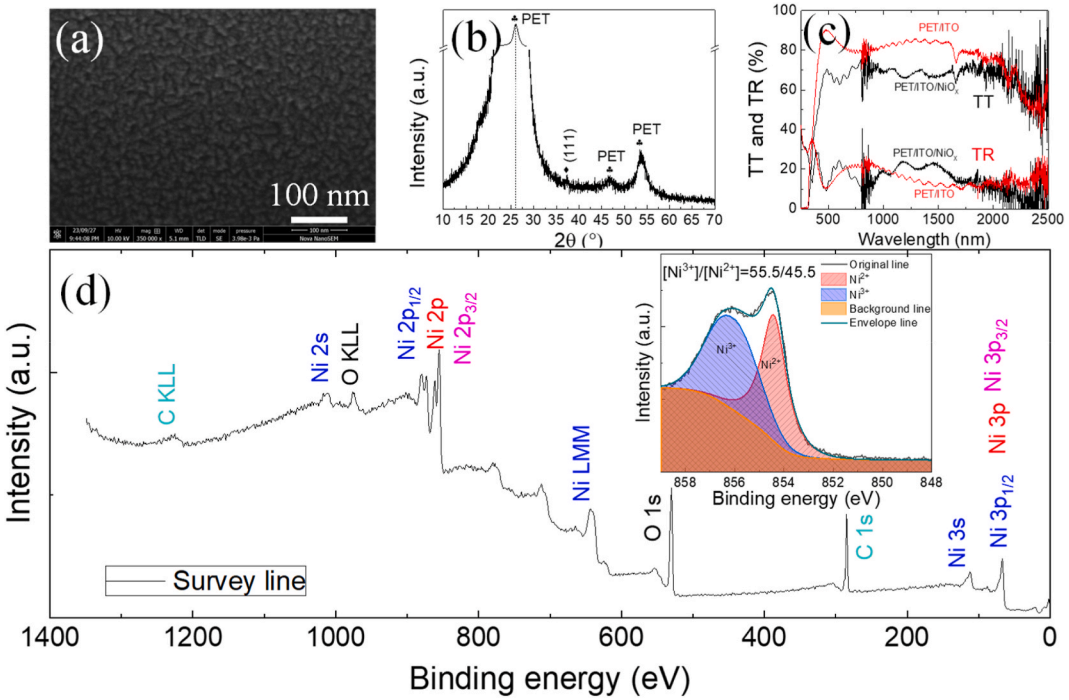

Fig. 2. The morphology (a), XRD patterns (b), optical TT and TR (c) as well as XPS results of reactively sputtered NiO_X thin films applied in the optimized flexible ATF-ECD.

As shown in Fig. 3(a), it is well found that the WO_3 exhibits relatively large and loose particles on the surface. A few boundaries in-between particles are clearly seen. As shown in Fig. 3(b), these WO_3 thin films prepared at the deflection points in the target voltage-O_2 flux curve shows a high transmission, an amorphous crystal structure and proper chemical compositions [27], which would be

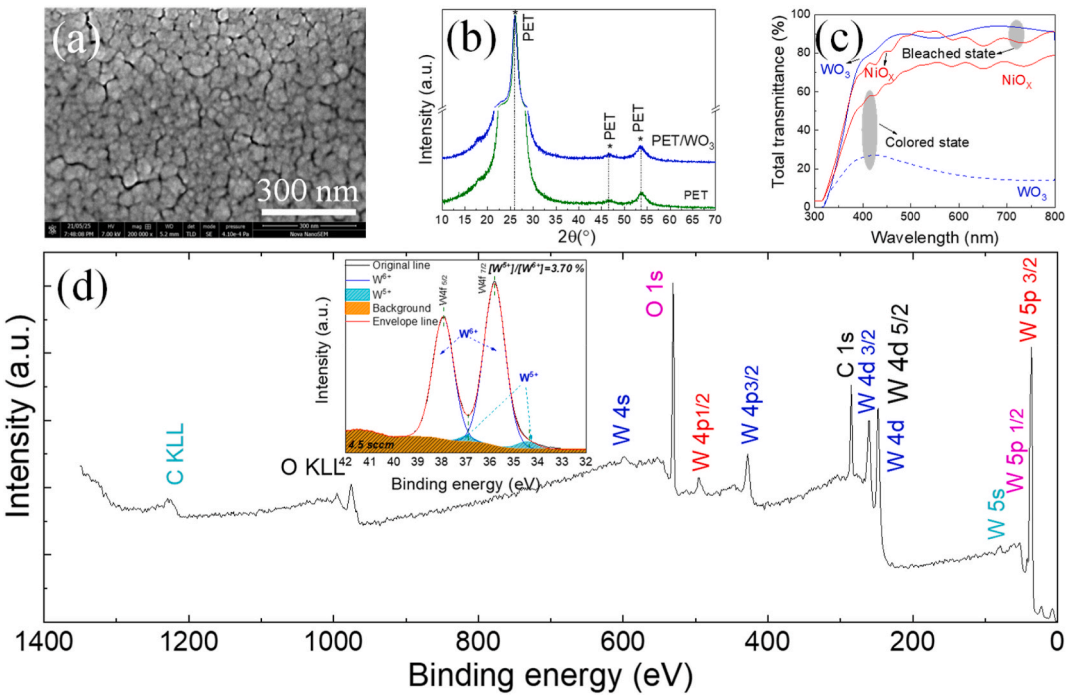

Fig. 3. The morphology (a), XRD patterns (b) and XPS results of reactively sputtered WO_3 thin films applied in the optimized flexible ATF-ECD. Moreover, the transmission spectra of PET/ITO/NiO_X and PET/ITO/WO_3 samples operated at bleached and colored state (c).

beneficial for the ion transports and following electrochromic properties. Similarly, Fig. 3(d) shows the survey curve of the WO_3 thin films and the high resolution scan curve of W core levels in the inserted figure. It is observed that a small amount of W^{5+} ions exist in the WO_3 thin films, which demonstrates that there are a small amount of the O vacancies for the charge neutrality. The $[W^{5+}]/[W^{6+}]$ ratio is only 3.7% and the O vacancies would be good for the carrier transfer as well. The diffusion coefficient of WO_3 is in the range of $(1–2.5) \times 10^{-10}$ cm^2/s) when they are measured in IM $LiClO_4$-PC solution, which is reported in our previous work [24]. Fig. 3(c) shows the transmission spectra of the PET/ITO/WO_3 at colored and bleached states. It is clearly observed that WO_3 thin films exhibited excellent electrochromic properties with wide optical modulation as well as with the high transparency at the bleached state and relatively low transmission at the colored state. Differently, the PET/ITO/NiO_X shows relatively small optical modulation, which is shown in Fig. 3(c). Their color is shallow brown at the colored state but highly transparent at the bleached state. As a matter of fact, the NiO_X mainly works as ionic storage layer in the high performance flexible ATF-ECDs with the device structure of PET/ITO/-NiO_X/$LiTaO_3$/WO_3/ITO here.

RF sputtered $LiTaO_3$ is normally prepared at room temperature and exhibits amorphous crystal structure with relatively small particles on the surface as shown in Fig. 1(d). The working pressure has a strong influence on the inner microstructure of the $LiTaO_3$, which leads to different carrier transfer properties. A low working pressure leads to a relatively compacted microstructure hindering carrier transfer while a high working pressure leads to a very low deposition rate causing a cost-efficiency problem. The optimized working pressure for preparing $LiTaO_3$ SE layer is about 3 Pa and the optimized film thickness is 200 nm in this study. As shown in the XRD pattern in Fig. 4 (a), the sputtered $LiTaO_3$ SE layer on the PET substrate also shows an amorphous crystal structure. Through the EIS measurement for the samples with the structured of the PET/ITO/$LiTaO_3$/Ag [29], the ionic conductivity of $LiTaO_3$ thin films could be analysed using the computer fitting according to the equivalent circuit as shown in Fig. 4 (b), where R1 is the series resistance related to the ITO and Ag layers, the R2 is related to the ionic conduction in $LiTaO_3$ while CPE1 (constant phase element) might be related to the double layer capacitance between the interfaces of ITO/$LiTaO_3$ and $LiTaO_3$/Ag and CPE2 might be related to a geometrical capacitance between electrodes [30,31]. Based on the fitting parameters, the ionic conductivity is calculated out to be 4.85×10^{-9} S/cm, which is inconsistent with the reported values [30,31].

When different voltages between −2 V and 3 V are imposed on the optimized flexible ATF-ECD during the coloring processes while keeping the same voltage at 3 V during bleaching processes, it is found that the optical modulation increases with the applied negative voltages. At a low driving voltage, the flexible ATF-ECD shows a relatively low TT@600 nm at the bleached state and relatively high

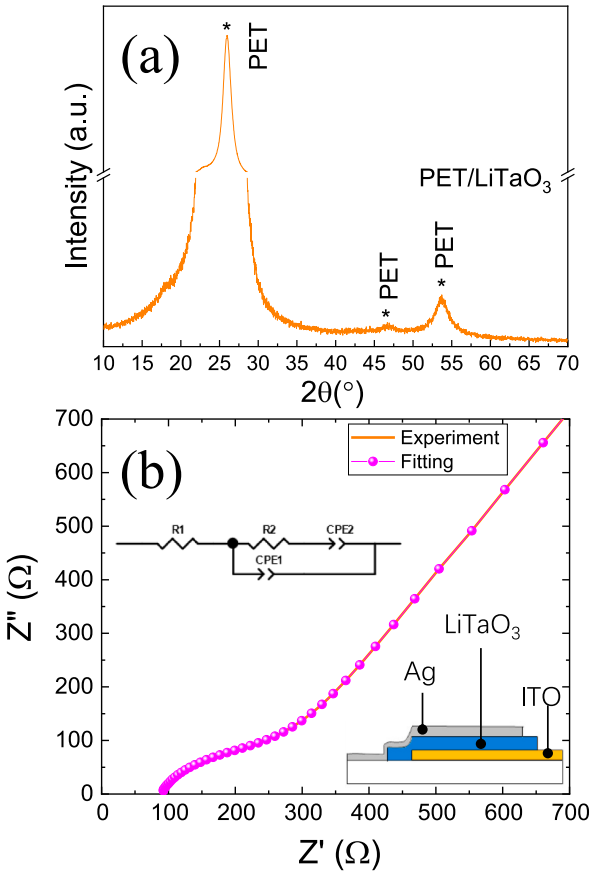

Fig. 4. The XRD pattern of the sputtered $LiTaO_3$ SE layer (a) and the EIS spectrum of the sample with the structure of PET/ITO/$LiTaO_3$/Ag (b). The insets show the structure and the equivalent circuit of the test sample.

TT@600 nm at the colored state. As the negative voltage reaches to −2.5 V the TT@600 nm at the colored state is decreased and at the same time the TT@600 nm at the bleached state is increased up to about 78.7%. Fig. 5 (b) shows the synchronous variations of the current density for these devices. It is clearly observed that the current density increases with the negative voltages during both bleaching and coloring processes. The detailed variations of the electrochromic parameters in a period for the flexible ATF-ECD with different driving voltages are exhibited in Fig. 6.

As shown in Fig. 6 (a), the electro-optical response (switching time) of the flexible ATF-ECD increases from 2.7 s to 7.1 s during the bleaching step and decreases from 14.1 s to 8.6 s, respectively, with the decreasing negative voltages from −2 V to −3 V. Fig. 6 (b) shows the corresponding current densities for the flexible ATF-ECD in this specific electrochromic periods during the CA measurements under different driving voltages, which increase with the negative voltages during the both bleaching and coloring steps. At the same time, the charge density varies very fast at the initial stage of the bleaching step and then keeps almost constant, which implies a complete discharge. Differently, it gradually increases with the time during the coloring step. Such phenomena are in agreement with the TT variations of the optical modulation as shown in Fig. 6 (a). Furthermore, it is found that the integrated charge density during coloring step is larger than that during bleaching step when the voltage is increased. The charge density in a coloring step is up to about 50 mC/cm^2 when the flexible ATF-ECD works under the lowest negative driving voltage of −3 V. The charge density ratio (or the charge density difference) i.e. Q_c (in a coloring step) to Q_b (in a bleaching step) ratio, gets larger with the decreasing negative voltages. The largest charge density ratio of 2.16 is obtained under the negative driving voltage of −3 V while it is almost 1 for the device under the negative driving voltage of −2 V. It might be related to the current leakage for the flexible ATF-ECDs during the coloring process under a much lower negative driving voltage. More details will be discussed in the following sections. The corresponding optical density difference (ΔOD) and coloration efficiency (CE) can be calculated out according to the following equations [23,32]:

$$\Delta OD = \ln\left(\frac{T_b}{T_c}\right) \tag{1}$$

$$CE = \frac{\Delta OD}{\Delta Q} \tag{2}$$

where the T_b and T_c are tested TT values at the bleached state and colored state, respectively, ΔQ charge density difference. As shown in Fig. 6 (e), ΔOD almost linearly varies with the charge density during the bleaching step. Differently, it linearly varies with the charge density at the initial period of the coloring step and then gradually increases with the increasing charge density as shown in Fig. 6 (f). Such a gradual increment in ΔOD with the charge density during coloring step demonstrates a low current utility efficiency i.e. a low CE, which is confirmed in Fig. 6 (h). The CE increases fast in the initial period to reaches to a peak value during coloring step and then decreases with the increasing charge density when the device works under a high driving voltage. Moreover, the CE decreases with the decreasing negative driving voltage over the whole coloring step. Differently, the CE exhibits relatively high values for the flexible ATF-ECD during all bleaching steps here as shown in Fig. 6 (g). The slight decrease of CE with the charge density at the post period of the bleaching step might be related with the deeply trapped Li^+ ions in the WO_3 layer, which are relatively difficult to be extracted out. More detailed would be discussed in the following sections.

Through the CV measurements it is found that the flexible ATF-ECD shows much larger current density with the voltage swept to lower negative values during the coloring process as shown in Fig. 7 (a). Moreover, it is observed that the complete discharge process in

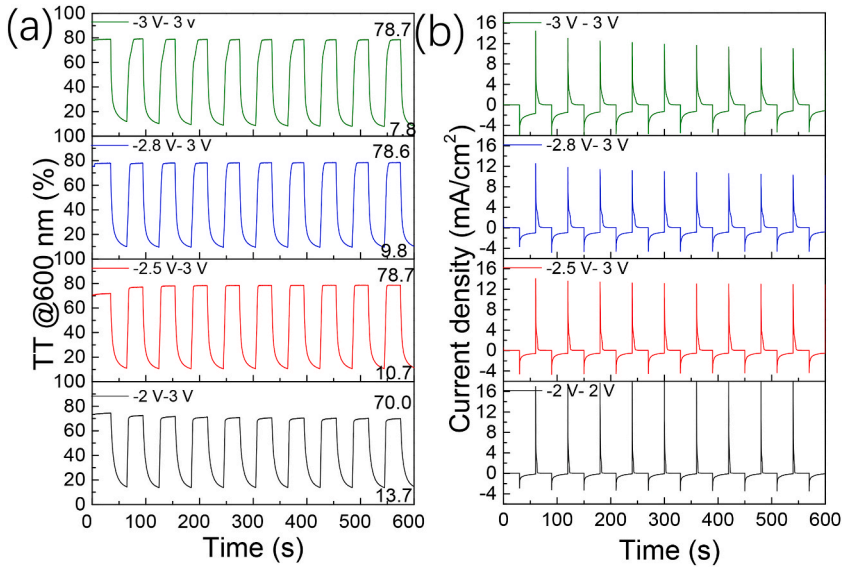

Fig. 5. The TT@600 nm (a) and current density (b) variations during CA measurements for the flexible ATF-ECD.

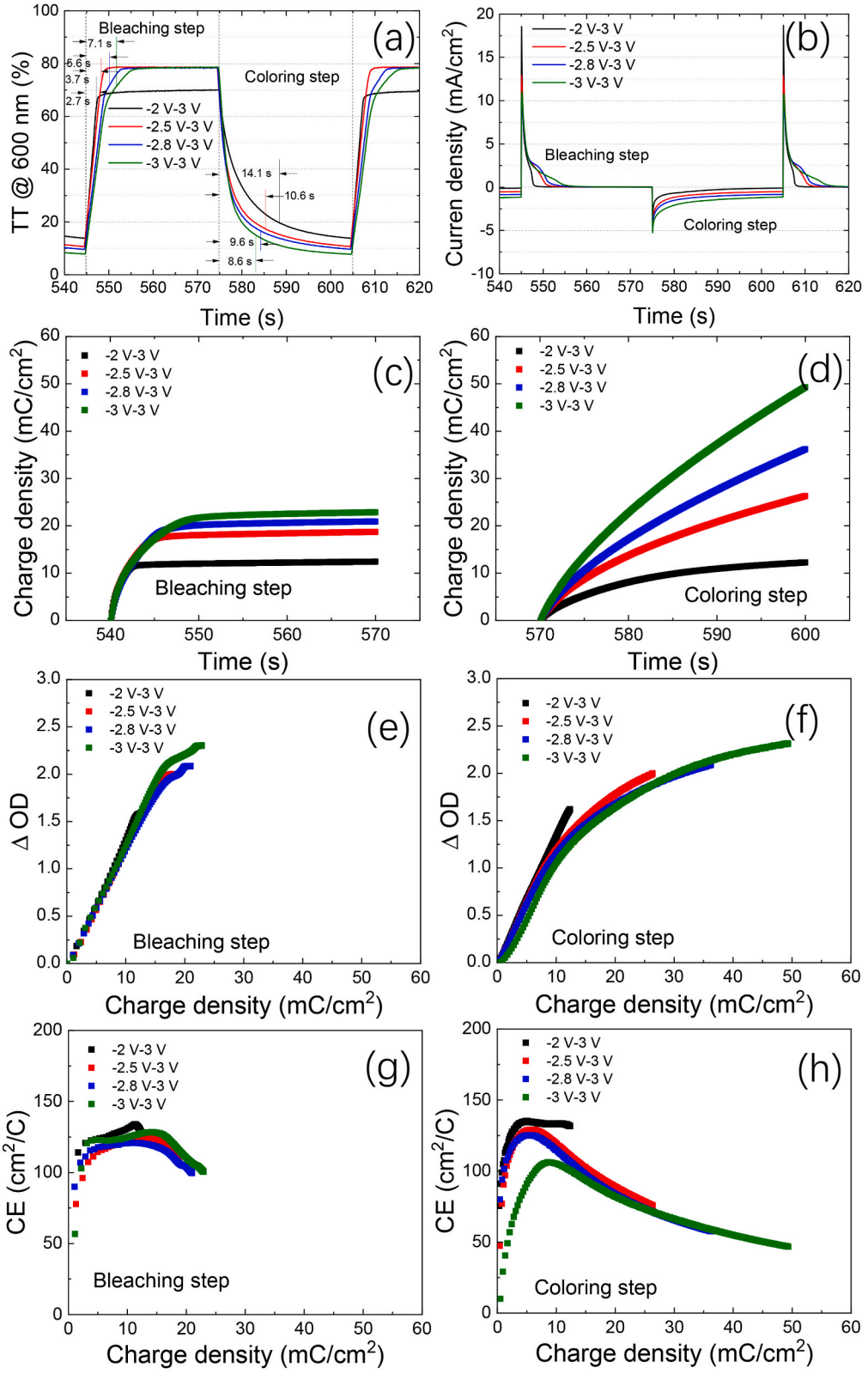

Fig. 6. The detailed electrochromic properties of the flexible ATF-ECD during CA measurements.

a bleaching process would be extended to the higher positive voltage. It demonstrates that some Li^+ ions deeply trapped in the EC layers during the coloring process must be extracted out under the higher voltages during the bleaching process. Moreover, the charge density during the coloring process in the CV measurement is larger than that during the bleaching process as shown in Fig. 7 (c and d). The charge density difference between coloring process and bleaching process gets larger with the negative driving voltages. Fig. 7 (b) shows the corresponding TT (@600 nm) variations during the CV measurements for the flexible ATF-ECD operated at different negative driving voltages. The lowest TT@600 nm decreases with the decreasing negative voltages. These observations are in accordance with the CA results as mentioned above.

The flexible ATF-ECD shows a relatively good open circuit memory (OCM), in which after 1000 s OCM process the TT@600 nm slightly increases from 12.9% to 18.4% after the coloring step under −2.5 V and from the 8.6%–15.9% after the coloring step under −3 V, respectively, as shown in Fig. 8 (b and d). The corresponding voltages in open circuit are changed from −2.5 V to −1.54 V and from −3 V to −1.53 V, respectively, as shown in Fig. 8 (a and c). Such degradation in OCM might be due to: (1) the inner Li atom out-diffusion from the EC layer because of the Li concentration difference inside; (2) the possible micro-shunt existed inside the flexible ATF-ECD, which is caused by the possible contaminations from some small particles during the whole preparation processes, leads the Li^+ ions and electrons to transfer inside the device under the established electromotive force (EMF). Actually, the thicker SE layers would reduce such a degradation in OCM [14]. In addition, the stacked multiple SE layers were also proved to be an effective device structure to enhance the OCM property [15,17].

Fig. 9 shows the transmission spectra of the flexible ATF-ECD at the bleached and colored states operated at different negative driving voltages. It is clearly observed that the flexible ATF-ECD at the bleached state shows rather high transmission over the whole wavelength range. The TT@600 nm for the ATF-ECD at the bleached state reaches to 79.4%. In the near infrared (NIR) wavelength range of 800 nm–2500 nm, the transmission is gradually decreased with the wavelength, which is mainly due to the light absorption. Moreover, the flexible ATF-ECD at the colored state exhibits rather low transmission over the whole wavelength range. The transmission of the flexible ATF-ECD decreases with the decreasing negative voltages. The TT@600 nm for the ATF-ECD at the bleached state operated at higher voltages between −2 V and −3 V reduces from 12% to 5.9%. The largest optical modulation of 73.5% has been achieved for this device. It is a great advantage for this kind of all-inorganic flexible ATF-ECDs possessing the ability to absorb the light over the whole wavelength range. It provides promising applications not only for the visible light modulation in the smart windows but also for NIR light modulation, filtering, sensing and etc. The inserted pictures in Fig. 9 show the appearances of the flexible ATF-ECDs at the bleached state and colored state, respectively. Moreover, a flexible ATF-ECD small module with a size of 10 cm × 10 cm has been prepared and shows a good cycling stability after 10000 s CA measurement with the durations of 45 s for each electrochromic step as shown in Fig. 10. The photographs on the right side of this figure exhibit the appearances of the small module at the bleached and colored sates.

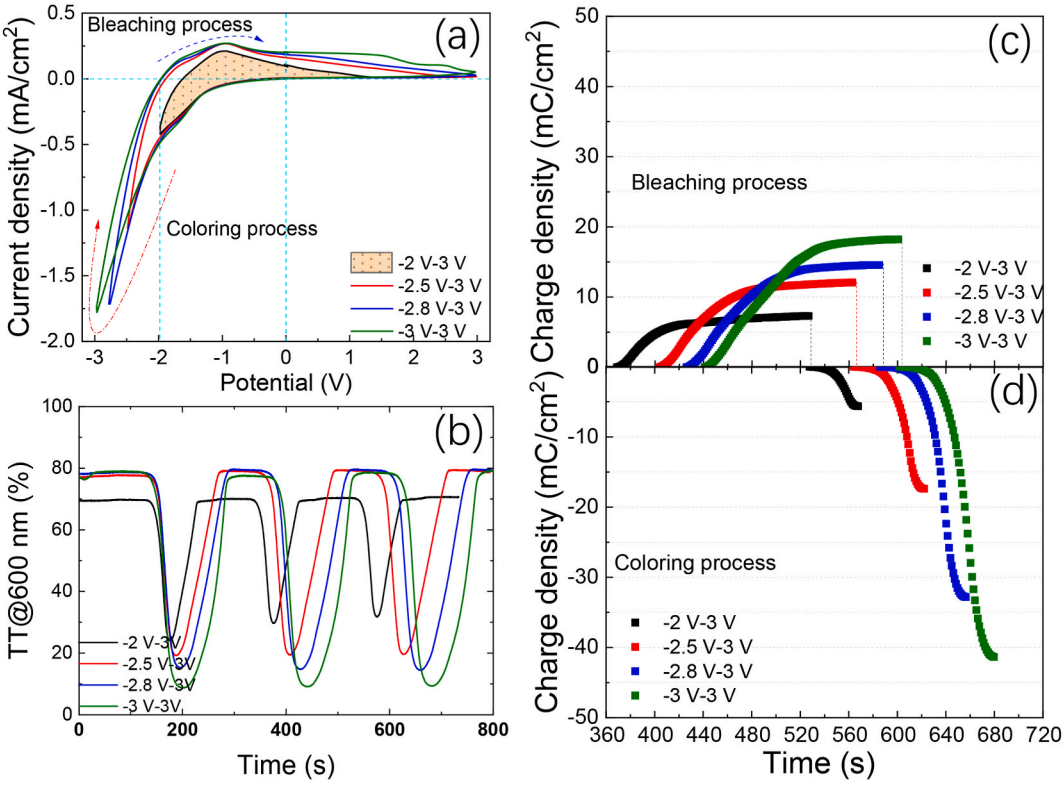

Fig. 7. The detailed electrochromic properties of the flexible ATF-ECD during CV measurements.

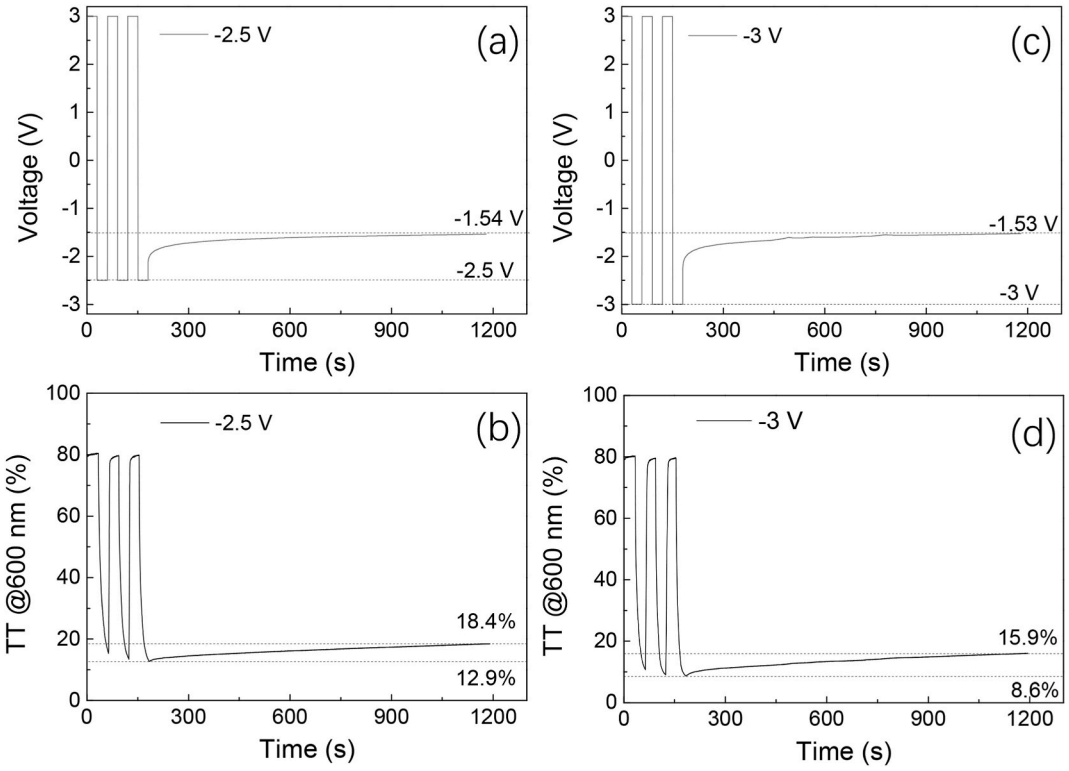

Fig. 8. The open circuit memory properties of the flexible ATF-ECD.

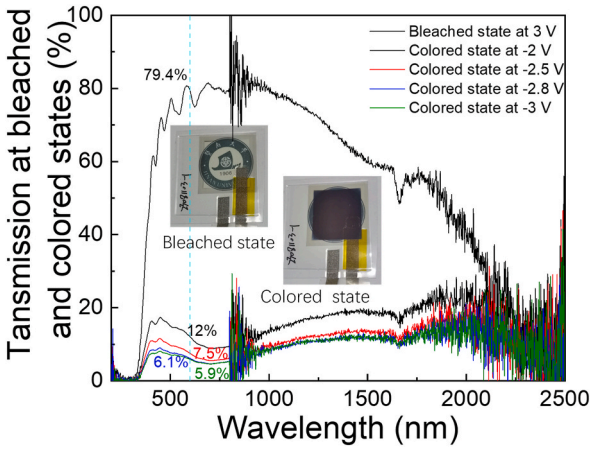

Fig. 9. The TT spectra at the bleached state (a) and colored state (b) for the flexible ATF-ECD applied with different driving voltages, in which the inserted photographs show the appearances of the device at the bleached and colored states, respectively.

Furthermore, Table 2 lists the electrochromic performance parameters of flexible ATF-ECDs reported by other researchers for comparison with the device in this work. In addition to the Li^+ based flexible ATF-ECDs, some researchers reported the flexible ATF-ECDs with H^+ as transport ion [5,8,27]. It is observed that Tang et al. reported a reverse device structure of PET/ITO/-WO_3/Nb_2O_5/$NiVO_X$/ITO [8], which is different from the normal flexible device configuration reported by other researchers. At the same time, they employed $NiVO_X$ as the IS layer and Nb_2O_5 as the SE layer, respectively. Our group reported the flexible ATF-ECDs with Ta_2O_5 SE layer (H^+ transport ions) achieving a relatively high optical modulation. Differently, Liu et al. reported Li^+ based flexible ATF-ECDs achieving an optical modulation of 65.2%@ 550 nm under a relatively high driving voltage (±4 V) [11]. Our flexible ATF-ECD in this work shows the increasing optical modulations from 56.3% to 70.9% @600 nm when it is operated at the decreasing negative driving voltages from −2.0 V to −3.0 V during the CA measurements as well as the relatively fast switching speeds for both bleaching and coloring steps.

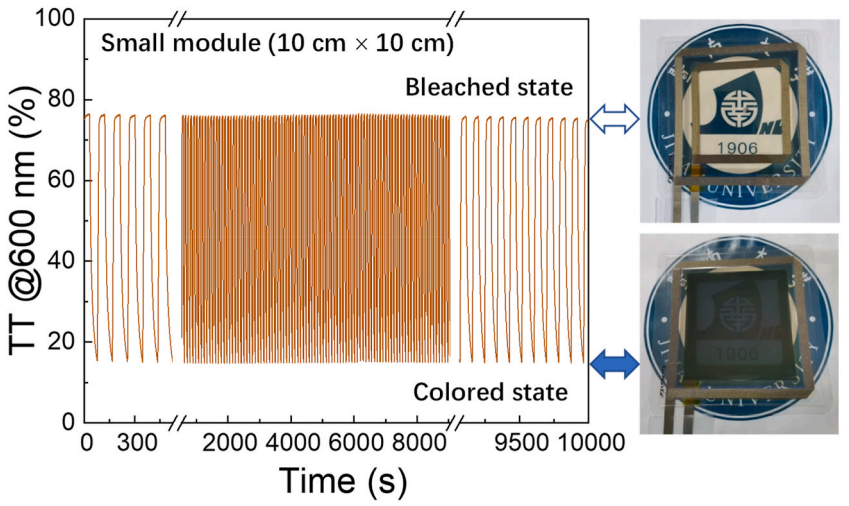

Fig. 10. The TT@600 nm during the CA measurement for a long timeof the flexible small module with a size of 10 cm × 10 cm (a) and the corresponding appearance photographs of the small module at bleached and colored state (b).

Table 2
The performance parameters of the reported flexible ATF-ECDs and the device in this work.

Configuration of Flexible ECD structure	Conduction type	Optical modulation (%)	τ_b (s)	τ_c (s)	Imposed voltage (V)	Reference
PET/ITO/WO_3/Nb_2O_5/$NiVO_X$/ITO	H^+	39@633 nm	5	6	±3	[8]
PET/ITO/NiO_X/Ta_2O_5:H/WO_3/ITO	H^+	60@550 nm	/	/	±2	[5]
PET/ITO/NiO_X/Ta_2O_5/WO_3/ITO	H^+	70.6@600 nm	2.2	15.6	±1.8	[27]
PET/ITO/NiO_X/$LiTaO_3$/WO_3/ITO	Li^+	65.2@550 nm	55	7	±4	[11]
PET/ITO/NiO_X/$LiTaO_3$/WO_3/ITO	Li^+	56.3@600 nm	2.7	14.1	−2.0 - (+3)	This work
		68.0@600 nm	3.7	10.6	−2.5 - (+3)	
		68.8@600 nm	5.6	9.6	−2.8 - (+3)	
		70.9@600 nm	7.1	8.6	−3.0 - (+3)	

Based on the observations above, it is found that the optimized flexible ATF-ECD with the highest optical modulation of 73.5% and relatively higher CE has been obtained. High negative driving voltages could effectively enhance the optical modulation. However, the high negative driving voltage such as −2.8 V and −3 V imposed on the flexible ATF-ECD during coloring processes would strongly lead to an increase in the charge density (or current density) and consequently the reduction of CE as shown in Figs. 6 and 7. A large part of charge density might belong to the leakage current i.e. pure electron current, which might be related to different electrical properties of the functional layers inside the ATF-ECDs and the specific device structure. As compared to the sandwich-type QSE-based ECDs (glass/ITO/NiO_X/QSE/WO_3/ITO/glass) [21,22], the ATF-ECDs normally have a very small ion conductivity (small ion concentration and low ionic mobility) and a small total thickness of the whole device. Thus, the transfer current will be strongly influenced by the inner electric field generated from the external voltages. It is well known that the current density (J) in ATF-ECDs depends on the ionic density (σ) in the electrolytes and applied electric field ($\varepsilon = V/d$). The charge density (Q) relies on not only the current density but also the specific surface area (denoted with A). The J and Q could be expressed as follows:

$$J = \sigma\varepsilon = qnu\frac{V}{d} \tag{3}$$

$$Q = JAt = \sigma\frac{V}{d}At \tag{4}$$

where q is the charge of carriers (ions and electrons), n carrier density, μ carrier mobility, V applied voltage, d the distance between the anode and cathode. A usually equals to 1 but strongly depends on the microstructure of the surface in some specific cases when the morphologies of some functional layers in the ATF-ECDs are varied. The ionic conductivity of the SE thin film might be only about 10^{-8} S/cm [30,31]. The thickness of $LiTaO_3$ SE layer is only a few hundred nanometres such as 200 nm here and the total thickness of NiO_X/SE/WO_3 is also a few hundred nanometres. Thus, when a high voltage is applied during the electrochromic process, the ATF-ECDs have a strong electric field inside. As a result, the current density and corresponding charge density will increase profoundly according to equations (3) and (4). Such a profound increment in current density mainly takes place in the coloring process. It should be noted that the ATF-ECD is similar to a solid state pseudo-capacitor [33–35], whose terminal voltage would linearly increase with the inner charged/discharged charges and the inner EMF would be established as well. For the normal case that the external voltage is

usually smaller than the maximal EMF, the established EMF will counterbalance to the external voltage and the coloring process (charging process) would be terminated. However, for the critical case when the coloring process is nearly completed but the external voltage (critical voltage V_c) is still larger than the inner EMF, the excess electron current would be generated. The main process is described as follows: when the coloring process is almost completed, the inner WO_3 phase is converted into the Li_XWO_3 phase, which has a good conductivity [36]. At the same time, the NiO_X phase and excited Li_ZNiO_X phase [37] have a relatively good conductivity as well. The excess external voltage imposed on the ATF-ECDs would form much stronger electric field and then generate the electronic current leakage (i'_{e^-}) even though there exists a relatively high dielectric but thin $LiTaO_3$ layer. This part of generated electronic current would destruct the Li^+ ion transfer channels inside the WO_3 and NiO_X layers, which is detrimental to the electrochromic stability of the ATF-ECDs. Moreover, the excess external voltage generates a very strong electric field, which forces the Li^+ ions to be deeply trapped in the WO_3 layer and finally results in a reduced TT at the bleached state and sometimes a decreased optical modulation. Both cases are schematically plotted in Fig. 11. In our case, the low negative voltage doesn't destruct the inner structure of these functional layers of the flexible ATF-ECD even though a relatively high leakage current generated, which is mainly due to good material properties of all functional layers prepared under excellent processes during the whole fabrication. Different from the case during the coloring process, the ATF-ECDs during the bleaching process have an increasing resistance, which is mainly due to the high resistant WO_3 phase and the other high resistant $Li_{Z+Y}NiO_x$. Even though a 3 V is applied on the flexible ATF-ECD during bleaching process, almost no current leakage is generated.

4. Summary

The monolithic, stacked flexible ATF-ECDs with excellent device performances have been prepared. The material properties and related interface properties with the optimized processes are also decisive to the comprehensive device performances. Besides, the proper test conditions in particular the driving voltage are especially important to achieve the best device performances for the ATF-ECDs. A low driving voltage would lead to a small optical modulation while a high driving voltage would result in a large optical

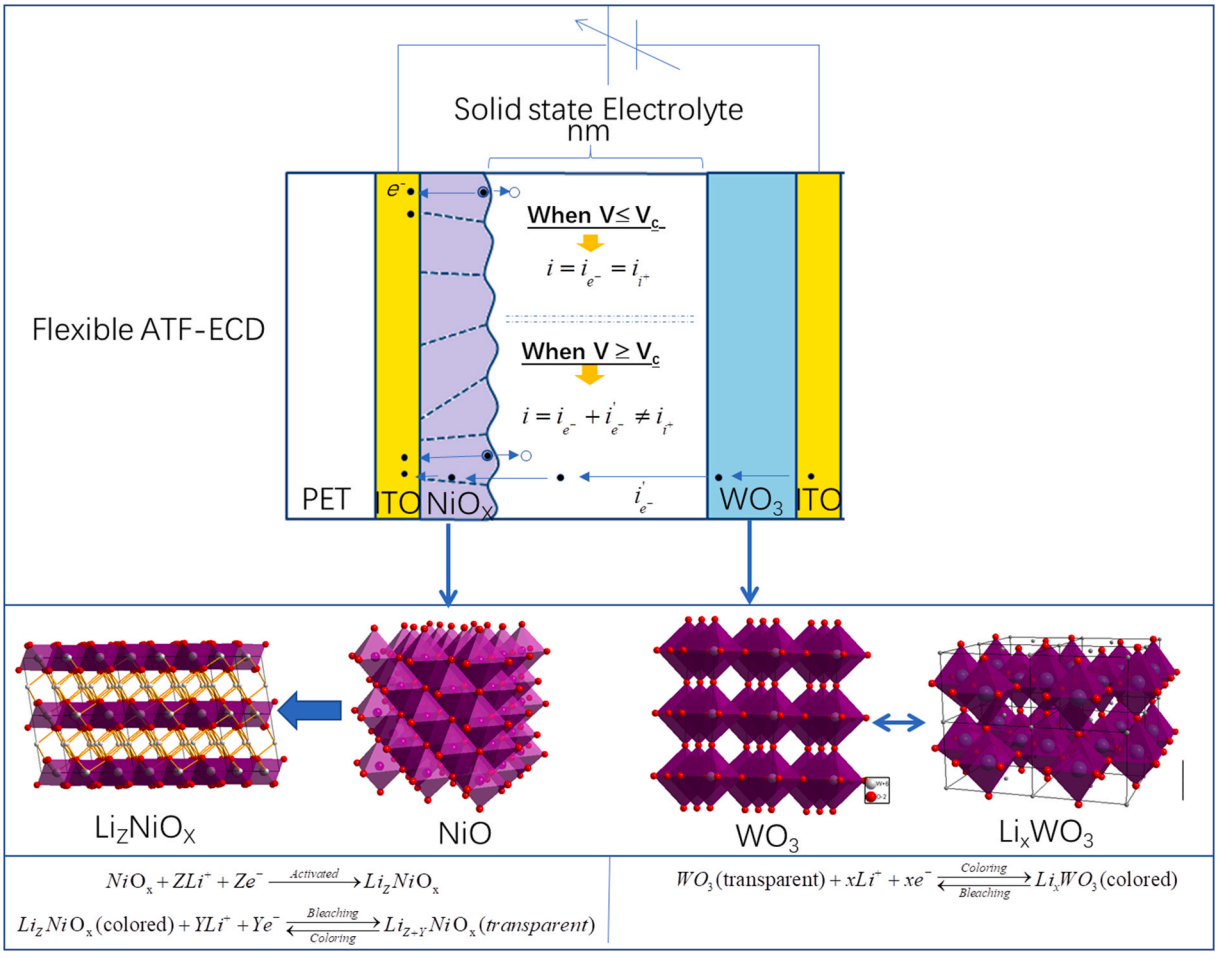

Fig. 11. The schematic of possible carrier transfer ways inside the flexible ATF-ECD operated under different driving voltages.

modulation, a fast electrical-optical response but may cause some problems such as current leakage, optical modulation degradation and even device destruction. In this study, the flexible ATF-ECD operated at −2.5 V during the coloring process and at 3 V during the bleaching process has achieved the best performances with high optical modulations (TT@600 nm) of 71.9% in static spectrum measurement and 68% in kinetic optical measurement, fast electrical-optical responses of 3.7 s during the bleaching process and 10.6 s during the coloring process. Relatively good OCM property is also presented after the coloring processes under −2.5 V and −3 V for the ATF-ECD even though the SE layer thickness and the whole device thickness are rather small. The flexible ATF-ECD with excellent device performances demonstrates the excellent material properties and the good process compatibility during the whole fabrications, which provides a promising application in the future smart window.

CRediT authorship contribution statement

Jinhong Ye: Writing – original draft, Validation, Methodology, Data curation. **Mingtao Chen:** Writing – original draft, Validation, Methodology, Data curation. **Hanyu Lu:** Validation, Methodology, Data curation. **Hongbing Zhu:** Writing – review & editing, Writing – original draft, Validation, Methodology, Investigation, Funding acquisition, Data curation, Conceptualization. **Meixiu Wan:** Writing – review & editing, Writing – original draft, Validation, Methodology, Investigation, Funding acquisition, Data curation, Conceptualization. **Kai Shen:** Validation, Methodology, Investigation, Funding acquisition. **Yaohua Mai:** Supervision, Resources.

Declaration of competing interest

The authors declare that they have no known competing financial interests or personal relationships that could have appeared to influence the work reported in this paper.

Acknowledgements

The authors would like to thank National Key R&D Program of China (No. 2022YFB4200701), Guangdong Basic and Applied Basic Research Foundation (No. 2023A1515010330), National Natural Science Foundation of China, China (no. 51903103, no. 61804064) and Guangzhou Beihuan Intelligent Transportation Co., Ltd (Beigao contract [2019] No. 89) for their financial supports of this work. The work is also supported by Guangdong Engineering Research Center of Thin-Film Photovoltaic Technology and Equipment is also acknowledged.

References

[1] C.G. Granqvist, M.A. Arvizu, İ. Bayrak Pehlivan, H.Y. Qu, R.T. Wen, G.A. Niklasson, Electrochromic materials and devices for energy efficiency and human comfort in buildings: a critical review, Electrochim. Acta 259 (2018) 1170–1182.
[2] S.D. Rezaei, S. Shannigrahi, S. Ramakrishna, A review of conventional, advanced, and smart glazing technologies and materials for improving indoor environment, Sol. Energy Mater. Sol. Cell. 159 (2017) 26–51.
[3] R.J. Mortimer, D.R. Rosseinsky, P.M.S. Monk, Electrochromic Materials and Devices, Wiley-VCH Verlag GmbH & Co. KGaA, 2015.
[4] X. Che, Z. Wu, G. Dong, X. Diao, Y. Zhou, J. Guo, D. Dong, M. Wang, Properties of all-thin-film glass/ITO/WO_3:H/Ta_2O_5/NiO_x/ITO electrochromic devices prepared by magnetron sputtering, Thin Solid Films 662 (2018) 6–12.
[5] D. Dong, W. Wang, G. Dong, F. Zhang, Y. He, H. Yu, F. Liu, M. Wang, X. Diao, Electrochromic properties and performance of NiO_x films and their corresponding all-thin-film flexible devices preparedby reactive DC magnetron sputtering, Appl. Surf. Sci. 383 (2016) 49–56.
[6] H. Lin, J. Ye, R. Wang, H. Zhu, M. Wan, K. Shen, Y. Mai, Tailoring the microstructure and chemical composition of Ta_2O_5 solid electrolytes for application in flexible ATF-ECDs, J. Alloys Compd. 918 (2022) 165723.
[7] R. Wang, L. Pan, Q. Han, H. Zhu, M. Wan, Y. Mai, Reactively sputtered Ta_2O_5 solid electrolyte layers in all thin film electrochromic devices, J. Alloys Compd. 865 (2021) 158931.
[8] C.-J. Tang, J.-M. Ye, Y.-T. Yang, J.-L. He, Large-area flexible monolithic ITO/WO_3/Nb_2O_5/$NiVO_\chi$/ITO electrochromic devices prepared by using magnetron sputter deposition, Opt. Mater. 55 (2016) 83–89.
[9] D. Dong, W. Wang, G. Dong, Y. Zhou, Z. Wu, M. Wang, F. Liu, X. Diao, Electrochromic properties of NiO_x:H films deposited by DC magnetron sputtering for ITO/NiO_x:H/ZrO_2/WO_3/ITO device, Appl. Surf. Sci. 357 (2015) 799–805.
[10] Y. Zhou, X. Diao, G. Dong, Z. Wu, D. Dong, M. Wang, Enhanced transmittance modulation of ITO/NiO_x/ZrO_2:H/WO_3/ITO electrochromic devices, Ionics 22 (2016) 25–32.
[11] Q. Liu, G. Dong, Y. Xiao, F. Gao, M. Wang, Q. Wang, S. Wang, H. Zuo, X. Diao, An all-thin-film inorganic electrochromic device monolithically fabricated on flexible PET/ITO substrate by magnetron sputtering, Mater. Lett. 142 (2015) 232–234.
[12] X. Song, G. Dong, F. Gao, Y. Xiao, Q. Liu, X. Diao, Properties of NiO_x and its influence upon all-thin-film ITO/NiO_x/$LiTaO_3$/WO_3/ITO electrochromic devices prepared by magnetron sputtering, Vacuum 111 (2015) 48–54.
[13] Y. Zhu, L. Xie, T. Chang, J. Bell, A. Huang, P. Jin, S. Bao, High performance all-solid-state electrochromic device based on Li_xNiO_y layer with gradient Li distribution, Electrochim. Acta 317 (2019) 10–16.
[14] Y. Xiao, G. Dong, J. Guo, Q. Liu, Q. Huang, Q. Zhang, X. Zhong, X. Diao, Thickness dependent surface roughness of sputtered $Li_{2.5}TaO_x$ ion conductor and its effect on electro-optical performance of inorganic monolithic electrochromic device, Sol. Energy Mater. Sol. Cell. 179 (2018) 319–327.
[15] Q. Huang, G. Dong, Y. Xiao, X. Diao, Electrochemical studies of silicon nitride electron blocking layer for all-solid-state inorganic electrochromic device, Electrochim. Acta 252 (2017) 331–337.
[16] Q. Liu, G. Dong, Q. Chen, J. Guo, Y. Xiao, M.-P. Delplancke-Ogletree, F. Reniers, X. Diao, Charge-transfer kinetics and cyclic properties of inorganic all-solid-state electrochromic device with remarkably improved optical memory, Sol. Energy Mater. Sol. Cell. 174 (2018) 545–553.
[17] Q. Liu, Q. Chen, Q. Zhang, G. Dong, X. Zhong, Y. Xiao, M.-P. Delplancke-Ogletree, F. Reniers, X. Diao, Dynamic behaviors of inorganic all-solid-state electrochromic device: role of potential, Electrochim. Acta 269 (2018) 617–623.
[18] Y. Zhao, X. Zhang, X. Chen, W. Li, L. Wang, Z. Li, J. Zhao, F. Endres, Y. Li, Preparation of Sn-NiO films and all-solid-state devices with enhanced electrochromic properties by magnetron sputtering method, Electrochim. Acta 367 (2021) 137457.
[19] Y. Zhao, X. Zhang, X. Chen, W. Li, Z. Li, M. Chen, W. Sun, J. Zhao, Y. Li, All-solid-state electrochromic devices based on the $LiAlSiO_4$ electrolyte, Mater. Lett. 292 (2021) 129592.

[20] Y. Zhu, L. Xie, T. Chang, A. Huang, P. Jin, S. Bao, Synergistic effect of Al^{3+}/Li^{+}-Based all-solid-state electrochromic devices with robust performance, ACS Appl. Electron. Mater. 2 (2020) 2171–2179.
[21] M. Da Rocha, Y. He, X. Diao, A. Rougier, Influence of cycling temperature on the electrochromic properties of WO_3//NiO devices built with various thicknesses, Sol. Energy Mater. Sol. Cell. 177 (2018) 57–65.
[22] X. Che, J. Guo, M. Wang, M. Wang, X. Zhong, Q. Liu, G. Dong, X. Wang, J. Yang, X. Diao, Thickness dependence of WO_3 and NiO_x thin films in all-solid-state complementary electrochromic devices, Energy Technol. 9 (2021).
[23] C.C. Granqvist, Handbook of Inorganic Electrochromic Materials, ELSEVIER SCIENCE B.V., Amsterdam - London - New York- Oxford - Paris - Shannon - Tokyo, 1995.
[24] L. Pan, Q. Han, Z. Dong, M. Wan, H. Zhu, Y. Li, Y. Mai, Reactively sputtered WO_3 thin films for the application in all thin film electrochromic devices, Electrochim. Acta 328 (2019) 135107.
[25] R. Wang, H. Lin, H. Zhu, M. Wan, K. Shen, Y. Mai, Preparation, investigation and application of nickel oxide thin films in flexible all-thin-film electrochromic devices: from material to device, J. Alloys Compd. 898 (2022) 162879.
[26] H. Lin, Z. Wang, Q. Han, R. Wang, L. Pan, H. Zhu, M. Wan, Y. Mai, The growth, properties and application of reactively sputtered nickel oxide thin films in all thin film electrochromic devices, Mater. Sci. Eng., B 270 (2021) 115196.
[27] R. Wang, H. Lin, H. Zhu, M. Wan, K. Shen, Y. Mai, A strategy of finely optimizing WO_X electrochromic layers for application in flexible ATF-ECDs, Electrochim. Acta 403 (2022) 139669.
[28] R.-T. Wen, C.G. Granqvist, G.A. Niklasson, Anodic electrochromism for energy-efficient windows: cation/anion-based surface processes and effects of crystal facets in nickel oxide thin films, Adv. Funct. Mater. 25 (2015) 3359–3370.
[29] M.J. Duggan, T. Saito, T. Niwa, Ionic conductivity of tantalum oxide by rf sputtering, Solid State Ionics 62 (1993) 15–20.
[30] L. Zhiyong, C. Xiaofeng, H. Xingfang, The preparation and ionic conductance of nano-amorphous thin film, J. Phys. Appl. Phys. 29 (1996) 2740.
[31] Y. Hu, V. Miikkulainen, K. Mizohata, T. Norby, O. Nilsen, H. Fjellvåg, Ionic conductivity in Li_xTaO_y thin films grown by atomic layer deposition, Electrochim. Acta 361 (2020) 137019.
[32] P. Ashrit, Transition Metal Oxide Thin Filmebased Chromogenics and Devices, Elsevier Ltd., 2017.
[33] Y. Jiang, J. Liu, Definitions of pseudocapacitive materials: a brief review, ENERGY & ENVIRONMENTAL MATERIALS 2 (2019) 30–37.
[34] S. Fleischmann, J.B. Mitchell, R. Wang, C. Zhan, D.-e. Jiang, V. Presser, V. Augustyn, Pseudocapacitance: from fundamental understanding to high power energy storage materials, Chem. Rev. 120 (2020) 6738–6782.
[35] L. Liu, K. Du, Z. He, T. Wang, X. Zhong, T. Ma, J. Yang, Y. He, G. Dong, S. Wang, X. Diao, High-temperature adaptive and robust ultra-thin inorganic all-solid-state smart electrochromic energy storage devices, Nano Energy 62 (2019) 46–54.
[36] Z. Mei, M. Wang, Y. Ding, X. Diao, Transmittance correlated real-time resistivity modulation and insulator-metal transition of electrochromic WO_3 thin films, Vacuum 214 (2023) 112219.
[37] S. Passerini, B. Scrosati, A. Gorenstein, The intercalation of lithium in nickel oxide and its electrochromic properties, J. Electrochem. Soc. 137 (1990) 3297–3300.